Electromagnetically Driven Soft Actuator

Federico Fries[1], Shuhei Miyashita[2], Daniela Rus[2], Rolf Pfeifer[3], and Dana D. Damian[4]

***Abstract*— Soft active elements will play a leading role in the development of dexterous and compliant robots. We present the fabrication of a soft functional material with ferromagnetic properties capable of producing compressive stress and strain in the presence of magnetic fields. The soft structure consists of a mixture of a super-soft elastomer and 99% pure iron powder. The magnetic and elastic properties of the material were modeled and investigated based on the principles of electromagnetism. These soft actuators reach up to approximately -2700 N/m^2 compressive stress when embedded in a solenoid coil running $7\,$A. Soft actuators were designed to achieve a strain of approximately 17% at $7\,$A. The soft actuators, with their unique capabilities, are promising for employment with soft robots, such as muscle-like structures or flexible actuators.**

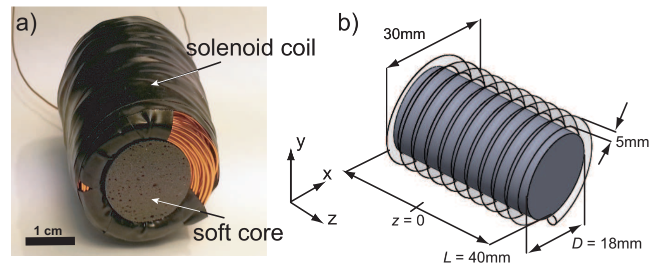

Fig. 1. Soft core electromagnet (SCEM). (a) Physical view. (b) Schematic view.

I. Introduction

Soft robotics has the potential of changing the way people interact with robots due to their intrinsic flexibility and safety [1]. An important challenge for advancing the field of soft robotics is the creation of soft actuators that can deliver a useful range of forces and torque, and accurate displacements.

A vast amount of work has been devoted to the design of muscle-like actuation to ascribe versatile mobility to robots [2]. Mechanisms for stiffness control have long been investigated [3] [4] [5], resulting in successful functional similarity to muscles, though most of them are rigid. An alternative to pure mechanical approaches for actuators is given by air-pressure technology [6] [7] [8], which introduces smooth robotic movements. McKibben actuators are flexible, lightweight, and widely used to actuate power-assisting devices for which compliance is required for safety [9]. Shape Memory Alloys (SMA) are also commonly used actuators for controlling stiffness, shape, or vibratory motions, but temperature modulation is necessary and may be difficult to achieve [10] [11]. Similar properties have also been engineered into polymers [12]. Jung et al. introduced dielectric elastomer actuators that deform (extend) in planar directions when voltage is applied to the attached compliant electrodes, due to electrostatic force [13]. An extension to holonomic six-degrees-of-freedom actuators was proposed by Conn et al. [14]. Relying on pneumatic technology, extension/contraction motions was achieved using origami-like structures embedded in elastomers, featuring inflatable chambers [15]. These advances enable new capabilities, though they require large actuators, or external pump attachments, and high power consumption.

In this paper, we propose ferromagnetic soft structures capable of actuation in the presence of the magnetic fields. In material engineering, ferrogels were created by mixing hydrogels with magnetic nanoparticles [16] [17] for medical applications such as drug delivery [18]. Magneto-elastomers have been investigated as well [19] [20]. Their work focused on elastic properties in the neighborhood of permanent magnets. Such magnetically sensitive elastomers can deform at room temperature and reversibly extend from $5-1000\%$ of the original volume.

The contributions of this paper are a novel soft actuator composed of an elastomer with ferromagnetic properties, modeling and fabrication process of the actuator, and extensive physical experiments to characterize the capabilities of the soft actuator. Electromagnetic-driven soft actuators have the potential to provide a combination of flexibility and high controllability at cm-scale, they can be used for low-profile soft robot applications, such as actuation devices in magnetic mediums or magnetic resonance imaging (MRI), as well as functional building blocks for soft robots. The proposed soft actuator is composed of a super-soft elastomer and iron powder, and represents a soft core (SC) caged in a solenoid copper coil referred to as a soft core electromagnet (SCEM), as in Fig. 1 . The actuation mechanism for the elastic structure relies on changing the external magnetic field, generated by the copper coil, which magnetizes the iron particles. In addition, the magnetized iron particles generate attraction forces between them, causing strain and stress of the volume of the SC. The principle of function is illustrated in Fig. 2.

The electromagnetic coil and the SC will be described and modeled in Section II. In Section III, the magnetic and elastic characteristics of the SC are investigated experimentally and compared with simulations. The results are evaluated and

[1]ZHAW Zurich University of Applied Sciences, Winterthur, Switzerland. [2]Computer Science and Artificial Intelligence Laboratory, Massachusetts Institute of Technology, U.S.A.. [3]University of Zurich, Switzerland. [4]Boston Children's Hospital, Harvard University, U.S.A.. Author for correspondence Dana D. Damian dana.damian@childrens.harvard.edu

discussed in Sections IV and V, while we conclude the study in Section VI.

II. System fabrication and modeling

In this section we introduce the components of the soft actuation system through fabrication and modeling.

A. Electromagnetic Coil System

For the windings of the electromagnet (EM), we used enameled copper wire with a diameter of $0.644\,\mathrm{mm}$ (AWG 22). A cylinder of almost identical size to the SC was built using rapid prototyping. The copper was wound separately around the cylinder, thus building a solenoid. After several preliminary trials with various winding numbers, we set the number of windings to $N = 500$ in order to ensure a strong magnetic flux density, starting with a relatively small amount of current flow (i.e., $0.75\,\mathrm{A}$). The measured resistance of the coil was $2.5\,\Omega$. Upon separation of the windings from the cylinder, the SC was transferred inside the coil (Fig. 1(a), building a SCEM.

The magnetic flux density B induced by the coil inside the SC can be considered homogeneous. The magnetic field along the z axis of a solenoid coil of length L, with the center at $L/2$ (Fig. 1(b)), can be described as

$$|B| = \frac{\mu_0 N I}{2L}\left[\frac{L+2z}{\sqrt{D^2+(2z+L)^2}} + \frac{L-2z}{\sqrt{D^2+(2z-L)^2}}\right], \tag{1}$$

where D is the diameter of the cylinder, N is the number of turns, I is the current, and μ_0 is the permeability of free space. For the magnetic flux density of the SC, μ_0 is replaced by $\mu = \mu_0 \cdot \mu_{rel}$, which is the magnetic permeability of the SC. The relative permeability μ_{rel} of the SCs was measured experimentally.

B. Elastomer-based SC

An SC was built by mixing and curing a super-soft elastomer (Ecoflex 00-10, Smooth On., Inc.) with 99% pure iron powder. The approximate diameter of an iron particle is $60\,\mu\mathrm{m}$. The iron powder concentration was increased up to $2.2 \cdot 10^3\,\mathrm{kg/m^3}$ and yet maintained the integrity of the cylindrical core. The iron powder occupies 60% of the entire volume. After a series of mechanical trials (e.g., stretching and twisting), the SC showed persistent elasticity and resilience to wear.

The diameter of the soft cylinder is $18\,\mathrm{mm}$ and the length was $40\,\mathrm{mm}$ (Fig. 1(b)). The Young's modulus E_0 of the soft core, derived from compression trials, was approximately $-3.5\,\mathrm{kPa}$, as recorded in the absence of the magnetic field. Ivaneyko et al. [21] modeled the elastic behavior of elastomeric lattices consisting of various distributions of magnetic particles. They found that, under the magnetic field, the elastomer lattice contracts and the Young's modulus varies depending on the magnetic field and the type of distribution of the iron particles. The mechanical behavior of the SC in a magnetic field can be studied using the equation of the free energy $F(\varepsilon)$ as a function of strain ε

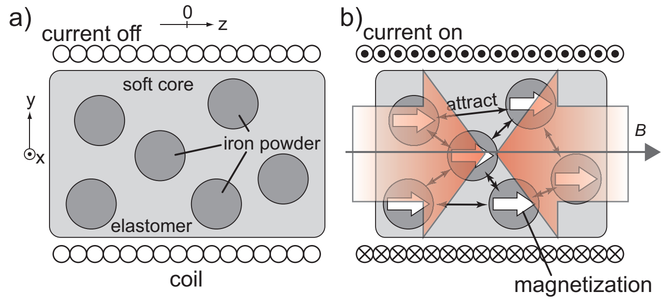

Fig. 2. Principle of SCEM. (a) Elastomeric core embedding iron powder resides inside copper windings. (b) Under a magnetic field generated by current application, the elastomer undergoes compressive stress and strain.

$$F(\varepsilon) = \frac{1}{2}E_0\varepsilon^2 + u(\varepsilon). \tag{2}$$

The magnetic term $u(\varepsilon)$ of Eq. (2) can be written as:

$$u(\varepsilon) = u_0\phi^2\left(\frac{M}{M_s}\right)^2 f(\varepsilon), \tag{3}$$

where the parameter $u_0 = \frac{\mu_0 M_s^2}{4\pi}$ defines the characteristic energy of the magnetic interaction, ϕ is the volume fraction of the particles, M is the magnetization, and M_s is the saturation magnetization of the SC. The dimensionless function $f(\varepsilon)$ has the following form:

$$f(\varepsilon) = -\alpha(1+\varepsilon)^{\frac{3}{2}} \sum_{i_x,i_y,i_z\neq 0} \frac{2\alpha^2(1+\varepsilon)^3 i_x^2 - i_y^2 - i_z^2}{[\alpha^2(1+\varepsilon)^3 i_x^2 + i_y^2 + i_z^2]^{\frac{5}{2}}}, \tag{4}$$

$f(\varepsilon)$ describes the sum of the attraction between all the particles contained in the SC. The index i represents the number of gaps between particles along the three axes. The distribution of the particles is considered isotropic [21], and therefore $\alpha = 1$. The magnetization M can be calculated with the magnetic field strength $H = \frac{B}{\mu}$ as follows:

$$M = \frac{M_s(\mu_{ini}-1)H}{M_s + (\mu_{ini}-1)H}, \tag{5}$$

with the magnetic permeability of the particles μ_{ini}.

The stress σ induced by the application of a magnetic field can be calculated by taking the first derivative of the free energy with respect to ε:

$$\sigma = -\frac{\partial F}{\partial \varepsilon}. \tag{6}$$

The equation tells that stress can be derived under the application of an external magnetic field.

III. Experimental setup and procedure

The characterization of the SC was realized by measuring the magnetic flux density, compressive stress, and strain utilizing the electromagnetic coil system. The default iron concentration in the SC was $2.2 \cdot 10^3\,\mathrm{kg/m^3}$, unless explicitly specified. This section describes the experimental setup used to measure these different quantities. Alternative core structures based on the magnetic behavior of the SC were designed in order to achieve actuation.

A. Magnetic Flux Density

The magnetic properties of the SC were investigated by measuring the magnetic flux density under direct current application. We used a Hall-effect sensor (Allegro A1302, sensitivity $k = 1.3\,\mathrm{mV/G}$, calibration $k = 1.2948\,\mathrm{mV/G}$) aligned to the center of the SCEM.

In the first experiment, the sensor was placed at a distance of 3 mm from the SCEM. The magnetic field was measured for eight values of the current, ranging from 0.75 A to 2.5 A. Three SC with different iron concentrations were fabricated for comparison: $1.1 \cdot 10^3\,\mathrm{kg/m^3}$, $1.6 \cdot 10^3\,\mathrm{kg/m^3}$, and $2.2 \cdot 10^3\,\mathrm{kg/m^3}$. Three trials of measurement were run for each condition.

In a second experiment, the SCEM was used to measure the magnetic flux density at nine positions offset from its end. For each offset, three different values of current were applied and simulated: 1.5 A, 2.25 A, and 3 A. Three trials of measurement for each position and current were conducted.

In a third experiment, we measured the magnetic field within the first 5 s of the application of current followed by 5 s of current removal, in order to quantify how fast the magnetization occurs in the SC. To demonstrate that the direction of the magnetic field can also be controlled, we ran the same experiment with the current flowing in the opposite direction. We ran five trials of measurements for each current value (i.e., ± 1 A and ± 3 A).

B. Compressive Stress and Strain

The elastic properties of the SC were investigated through a number of stress and strain experiments. Stress was derived by measuring the force inside the SC. The SCEM was placed horizontally. We used a force-sensitive resistor (FSR) sensor (Interlink Electronics, Inc.) placed in the center of the SC, parallel to the base of the cylindrical core and perpendicular to the magnetic field. The FSR was inserted in a small transversal cut made at the center of the core. The signals from the sensor were acquired using a data acquisition system (Data Acquisition System, National Instruments) through Labview (National Instruments) at 1000 Hz, and they were further processed in Matlab (Mathworks). Strain was measured at the same time by monitoring the horizontal displacement against a ruler placed on the back of the solenoid coil. A camera recorded the experiment, and the displacement was determined using the software Tracker [22]. These stress and strain experiments were conducted through the short-term application and removal of external magnetic fields in five trials. Compressive stress and strain were measured for seven values of current, ranging from 1 A to 7 A, recorded for periods of 3 s.

C. Actuation

In order to achieve an increased actuation of the SC, the structure was modified as shown in Fig. 3. The SC was segmented into smaller hollow cylinders of size $6 \times 2 \times 4$ mm (outer radius $\times$ inner radius $\times$ height) connected by hexagonal-shaped linkages. The hollow cylinder cores had the same iron concentration as the core described previously ($2.2 \cdot 10^3\,\mathrm{kg/m^3}$). The hexagonal-shaped linkages were built from elastomer (Ecoflex 00-30, Smooth On., Inc.). The size of the linkage was $1 \times 6 \times 2$ mm (width $\times$ diameter $\times$ length) (Fig. 3(a)). The lateral sides of the elastomeric linkage had a built-in $4\,\mathrm{mm^2}$ paper layer to prevent compressive strain under the weight of supporting structures. Embedding paper structures into elastomeric matrices offers many possibilities for programming the mechanical properties of the resulting composites [23]. We built three types of SCs (Fig. 3(d)), the strain was measured using the experimental setup in Fig. 3(b). The SC was placed inside the coil vertically. A wooden ruler bar was placed through the hole of the SC to indicate the vertical displacement of the SC at various currents generated through the coil. A camera recorded both experiments, and the displacement was measured using the software Tracker.

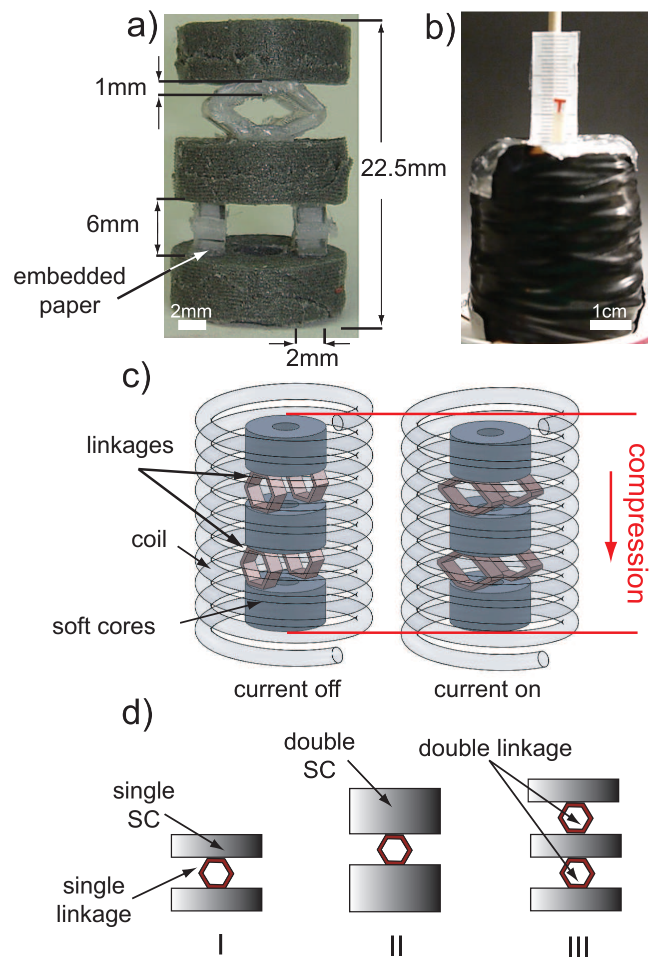

Fig. 3. Soft cores for actuation. (a) SC featuring two layers of linkages. (b) Experimental setup for the measurement of strain of the SC. (c) Schematics of the SC for strain generation. (d) Different SC structures: I) a single SC with one linkage layer, II) a double SC with one linkage layer, III) an SC with two linkage layers.

IV. Experimental Results of the SC

This section presents the results of the experiments described in the previous section.

A. Magnetic Flux Density

The results of the first experiment, in which the magnetic flux density was recorded at 3 mm from the SCEM with differing concentrations of iron powder, are presented in Fig. 4. Regardless of the applied currents, a linear relationship existed between the current and the magnetic field. As expected, the plot indicates that the higher the concentration of iron, the higher the magnetic field flux density through the cores. Furthermore, larger iron powder concentrations increased the slope of the linear relation between the magnetic flux density and applied current. Given the slope of the computed data fitting, the relative permeability $\mu_{rel} = 1.2$ was extracted for the SC with $2.2 \cdot 10^3$ kg/m^3 concentration of iron powder, implying that the SC is capable of increasing the magnetic flux density.

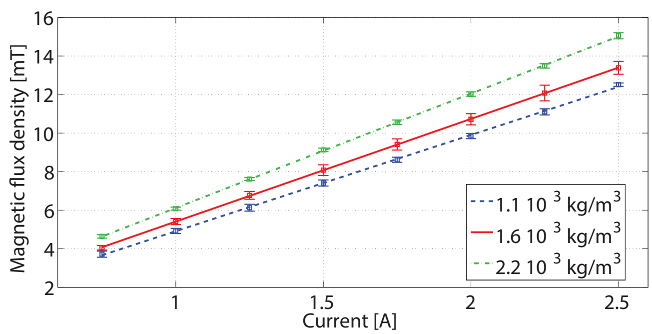

Fig. 4. Magnetic flux density of three SCs, depending on their iron concentrations and applied current. The average and standard deviation were computed over three trials.

The magnetic flux density depending on the distance from the EM is shown in Fig. 5, as experimentally measured and as modeled using Eq. (1) and μ_{rel}. The plot shows the average of the three conducted trials for each condition. The standard deviation was smaller than 0.044 mT. For the three currents applied, the magnetic field measurements were reasonably predicted by the model.

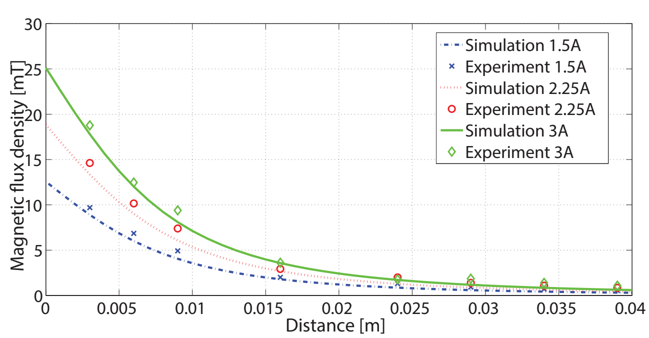

Fig. 5. Experimental and theoretical magnetic flux density for the SC at three currents and various distances from the SCEM, as measured by a Hall-effect sensor. One data point represents the average of three trials.

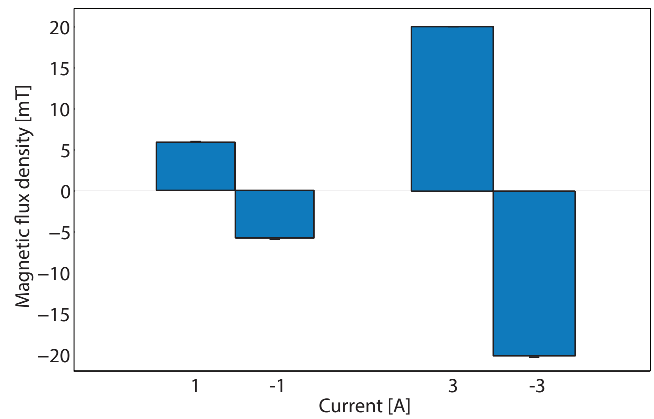

Fig. 6. Magnetic flux density of the SC under ± 1 A (± 3.2 V) and ± 3 A (± 8.7 V). The average and standard deviation were computed over five trials.

The magnetic flux density recorded in the third experiment, in which the activation and the direction of the magnetization were changed, is shown in Fig. 6. The experiment demonstrates that the amount and direction of the magnetic field in the SCEM can be regulated. It also shows that the magnetic field is induced immediately after the current is applied.

B. Compressive Stress and Strain

Due to its ferromagnetic and elastic properties, the SC exhibits a unique behavior (i.e., compressive stress and strain). The compressive stress has the same orientation as the induced magnetic field. This behavior is reported and modeled in a number of theoretical studies [21] [24]. The compressive stress and strain of the SC measured by short-term application of current is presented in Fig. 7. The SC started to show the elastic characteristics under the application of 3A of current. For this reason, only six measurements are shown in the plot. In this case, the SC can reach a relative stress of up to -2700 N/m^2 after magnetization occurs and a strain of $5.5 \cdot 10^{-3}$ under the application of 7 A. Based on Eq. (6), a linear fit was chosen. To compare the measurement, the stress was simulated for measured strain points, and a linear fit was made. Different parameters were needed for the simulation of stress (Eq. (4)). The values describing the magnetic properties of the iron particles were chosen according to [25]. The magnetization for carbonyl iron particles of the size 2 μm was estimated to be $M_s \approx 1990$ kA/m and a magnetic permeability of $\mu_{ini} = 132$. The slight disagreement between the simulated stresses and the corresponding measurements can be explained by the selection of the values for the simulation. This topic will be further elaborated in the discussion section.

The results given by the experiment demonstrate that both stress and strain performed by the SC are caused by the external magnetic field induced by the EM. They furthermore they indicate that the control of the strain and stress of the SC can be accomplished by altering the external magnetic field.

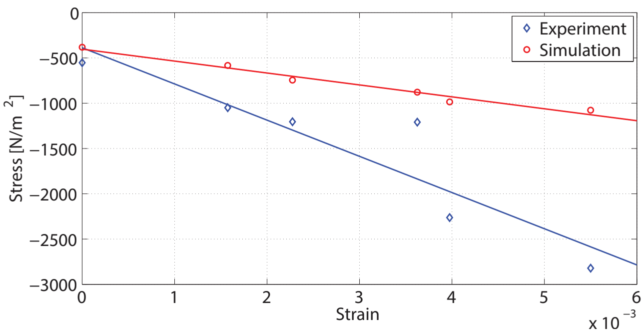

Fig. 7. Measure and simulation of stress according to strain. Strain and stress measured simultaneously for currents of 1 to 7 A. Corresponding linear fit are represented by solid lines. One data point represents the average of 5 trials.

C. Actuation

A unique feature of the SCs is the strain that occurs under the presence of the magnetic field. Fig. 8 shows the strain capabilities of different structures designed to achieve larger actuation. The SC features three types of structures, as described in Fig. 3(d). Regardless of the structure of the SCs, strain has a non-linear increase with respect to the current flow. Differing types of structures change the strain rates. The SCs start to compress at 2.5 A. The highest rates of strain were recorded by the SC structure that features a single SC and two linkage layers (Fig. 3(d)III), reaching a strain of approximately 17% at 7 A. The structures featuring one layer of linkages (Fig. 3(d)I and (d)II) had less strain, since the magnetic force of the cores was weaker.

The non-linearity of the curves was due to both the magnetic field and the non-linear spring function of the hexagonal linkages. Once the linkage starts to bend vertically, less force is needed to strain the core. This explains the increased non-linearity of the strain recorded by the third structure relative to the first structure.

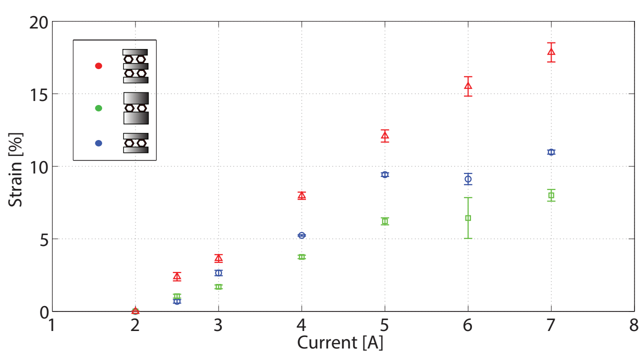

Fig. 8. Compressive strain measured on three different SC structures. Averages and standard deviations were computed over five trials for each experimental condition.

D. Proof of concept

A stamping application was designed to demonstrate the actuation capabilities of the SC. The SC is an ideal actuator to perform stamping, since delicate and fast actuation is needed. A single soft cylinder with a two linkage layer structure (Fig. 3(d)III) was chosen to perform this experiment. A stamp made of rubber foam with red ink was attached to the SC, and the core was placed vertically inside the copper solenoid coil. The SC was positioned in such a way that a part of it was outside the coil as shown in Fig. 9(a). In this case, the initial state was a compressed SC, which means that current was turned on at a value of 6 A, generating a displacement of 2.85 mm. A piece of paper was attached to a wooden plate and positioned over the SC at a considerable distance, far enough to let the SC decompress and push the stamp against it (Fig. 9(b)). In the second step, the current was turned off to release the compressed SC (Fig. 9(c)). In order to separate the stamp from the paper, the SC was compressed for a brief moment by turning the current on releasing the soft actuator against the wooden plate. Finally, the stamp can be seen in Fig. 9(d).

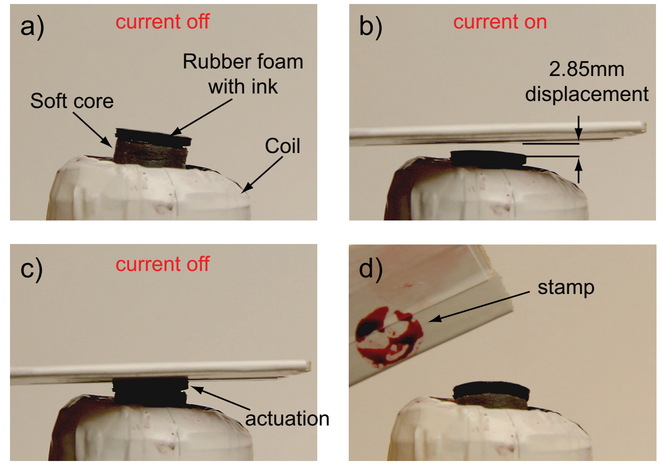

Fig. 9. Stamping demonstration. (a) SC and stamp with red ink is attached to the core. (b) Current turned on, displacement is generated. (c) Current is turned on performing actuation (d) Ink is transmitted to the piece of paper.

V. Discussion

In this section we discuss general remarks about the electromagnetically driven soft actuator.

A. Electromagnetic Coil System

The capabilities of the solenoid coil built for our experiment are strongly connected to the choice of the copper wire. The results of the magnetic field induced by the coil may vary depending on the capacity and width of the wire and the number of turns in the coil. Magnetic fields can be achieved in many ways (e.g., Helmholtz coils). An entire SCEM can be built by building a soft coil, as in [26], though the magnetic field will be significantly weaker.

High amounts of current were used in our experiments, increasing the solenoid coils temperature significantly, from 26°C to 32°C in 30 s of 3 A current flow. For this reason, actuation should be considered for short amounts of time.

B. Elastic behavior measurements

The SC model presented in Section II required various parameters, including the number of particles inside the

SC along the axis, the distance between particles, and the permeability of the particles, etc. Values characterizing the magnetic properties of particles were taken from [25], which describe carbonyl-iron particles of similar sizes. Parameters regarding the SCs, such as the number of gaps and the distance between particles, were calculated based on weight, concentration, the density of the soft elastomer and the size of the cores. To test the connection between these values and the results, several simulations were performed in which these values were varied in a specific range. The results showed that any change in the values could produce diverse outputs. We focused on comparing the simulations with our measurements, therefore the parameters chosen were similar to the parameters of our SC.

VI. Conclusions and Future Research

We developed a novel electromagnetically driven soft actuator, and investigated its characteristics and potential for robotics. The results of the experiments indicate the ability of the SCs to output stress and strain by altering an external magnetic field. Modifying the structures of the SC allowed considerable actuation. The SCs have the potential to be used as functional and structural building blocks for robots, and their actuation can be regulated according to the magnetic field applied. Our future work will pursue an all-soft electromagnet, replacing the cooper wire with a stretchable origami coil investigated in our group [26]. We also intend to improve the elastic and magnetic properties of the soft EM to provide scalability and enhaced flexibility.

Acknowledgment

Support for this work has been provided partially by NSF grants 1240383 and 1138967, and the SNF fellowship grants PBZHP2-135917 and PBZHP2-133472.

References

[1] C. Majidi. Soft robotics a perspective: Current trends and prospects for the future. *Soft Robotics*, 1:5–11, 2013.

[2] R. Van Ham, T.G. Sugar, B. Vanderborght, K.W. Hollander, and D. Lefeber. Compliant actuator designs. *IEEE Robotics and Automation Magazine*, pages 81–94, 2009.

[3] S.A. Migliore, E.A. Brown, and S.P. DeWeerth. Biologically inspired joint stiffness control. In *IEEE International Conference on Robotics and Automation (ICRA)*, pages 4508–4513, 2005.

[4] G. Tonietti, R. Schiavi, and A. Bicchi. Design and control of a variable stiffness actuator for safe and fast physical human/robot interaction. In *IEEE International Conference on Robotics and Automation (ICRA)*, pages 526–531, 2005.

[5] H.V. Quy, L. Aryananda, F.I. Sheikh, F. Casanova, and R. Pfeifer. A novel mechanism for varying stiffness via changing transmission angle. In *IEEE International Conference on Robotics and Automation (ICRA)*, pages 5076–5081, 2011.

[6] D.G. Caldwell, G. Medrano-Cerda, and M. Goodwin. Control of pneumatic muscle actuators. *IEEE Control Systems Magazine*, 15(1):4017–48, 1995.

[7] G.K. Klute, J.M. Czerniecki, and B. Hannaford. Mckibben artificial muscles: Pneumatic actuators with biomechanical intelligence. In *IEEE/ASME International Conference on Advanced Intelligent Mechatronics*, pages 221–226, 1999.

[8] B. Tondu and P. Lopez. Modeling and control of mckibben artificial muscle robot actuators. *IEEE Control Systems*, 20(2):15–38, 2000.

[9] S. Kuriyama, M. Ding, Y. Kurita, T. Ogasawara, and J. Ueda. Flexible sensor for mckibben pneumatic actuator. In *Sensors*, pages 520–525, 2009.

[10] V. Birman. Review of mechanics of shape memory alloy structures. *Appl. Mech. Rev.*, 50(11):629–645, 1997.

[11] B.S. Balapgol, S.A. Kulkarni, and K.M. Bajoria. A review on shape memory alloy structures. *International Journal of Acoustics and Vibration*, 9(2):6117–68, 2004.

[12] A. Lendlein and S. Kelch. Shape-memory polymers. *Angew. Chem. Int. Ed.*, 41:2034–172057, 2002.

[13] K. Jung, K.J. Kim, and H.R. Choi. Self-sensing of dielectric elastomer actuator. *Sensors Actuators A: Physical*, 143:343–351, 2008.

[14] A.T. Conn and J. Rossiter. Towards holonomic electro-elastomer actuators with six degrees of freedom. *Smart Mater. Struct.*, 21:035012, 2012.

[15] R.V. Martinez, C.R. Fish, X. Chen, and G.M. Whitesides. Elastomeric origami: Programmable paper-elastomer composites as pneumatic actuators. *Advanced Functional Materials*, 22:1376–1384, 2012.

[16] M. Zrínyi, L. Barsi, and A. B˝uki. Ferrogel: a new magneto-controlled elastic medium. *Polimer Gels and Networks*, 5:415–427, 1997.

[17] R. Fuhrer, E. K., N. A. Luechinger, and W. J. Stark. Crosslinking metal nanoparticles into the polymer backbone of hydrogels enables preparation of soft, magnetic field-driven actuators with muscle-like flexibility. *Small*, 5(3):383–388, 2009.

[18] J. Dobson. Magnetic nanoparticles for drug delivery. *Drug Development Research*, 67:55–60, 2006.

[19] Z. Varga, G. Filipcsei, and M. Zrínyi. Magnetic field sensitive functional elastomers with tuneable elastic modulus. *Polymer*, 47:227–233, 2006.

[20] M.R. Jolly, J.D. Carlson, and B.C. Munoz. A model of the behaviour of magnetorheological materials. *Smart Mater. Struct.*, 5:607–614, 1996.

[21] D. Ivaneyko, V.P. Toshchevikov, M. Saphiannikova, and G. Heinrich. Magneto-sensitive elastomers in a homogeneous magnetic field: A regular rectangular lattice model. *Macromolecular Theory and Simulation*, 20:411–424, 2011.

[22] D. Brown. Tracker video analysis and modeling tool. http://www.cabrillo.edu/ dbrown/tracker/, December 2009.

[23] Ramses V. Martinez, Carina R. Fish, Xin Chen, and George M. Whitesides. Elastomeric origami: Programmable paper-elastomer composites as pneumatic actuators. *Advanced Functional Materials*, 22:1376–1384, 2012.

[24] L. Borcea and O. Bruno. On the magneto-elastic properties of elastomer-ferromagnet composites. *Journal of the Mechanics and Physics of Solids*, 49:2877–2919, 2001.

[25] G. Bossis, C. Abbo, S. Cutillas, S. Lacis, and C. Metameyer. Electroactive and electrostructured elastomers. *International Journal of Modern Physics B*, 15:564–573, 2001.

[26] S. Miyashita, L. Meeker, M. Goeldi, Y. Kawahara, and D. Rus. Self-folding printable elastic electric devices: Resistor, capacitor, and inductor. In *IEEE International Conference on Robotics and Automation (ICRA)*, accepted.